Final Report

ynamics

Università degli Studi di Padova

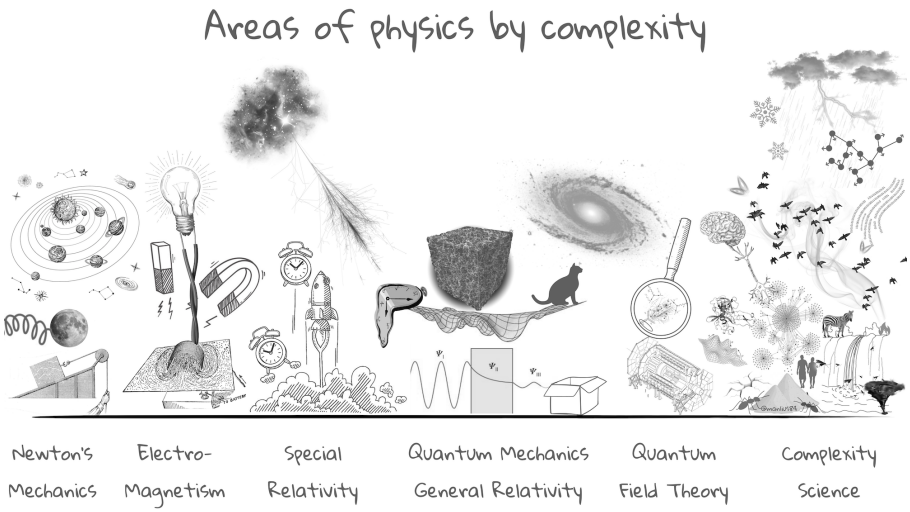

Project 18: Turing patterns

Project 41: Public transport in large cities worldwide

Waruszynski Sebastian

Last update: January 30, 2026

Contents

1 | Reproduction of Turing Patterns on Complex Networks

Task leader(s): *Your Name*

This report documents my reproduction of the seminal results by Nakao and Mikhailov. I have implemented the Mimura-Murray reaction-diffusion model on various network topologies (BA, ER, and SBM) to investigate how the interplay between kinetics and spectral properties leads to localized stationary patterns.

1.1 | Mathematical Framework

I analyzed a system of N nodes where each node i contains an activator u_i and an inhibitor v_i. The dynamics are defined by:

$$\frac{du_i}{dt} = f(u_i, v_i) + \epsilon \sum_{j=1}^{N} L_{ij} u_j, \quad \frac{dv_i}{dt} = g(u_i, v_i) + \epsilon\sigma \sum_{j=1}^{N} L_{ij} v_j$$

where $L_{ij} = A_{ij} - k_i \delta_{ij}$ is the network Laplacian, ϵ is the coupling strength, and σ is the diffusion ratio. For the Mimura-Murray kinetics, the Jacobian $\mathbf{J}$ at the fixed point $(\bar{u}, \bar{v})$ determines the stability. the critical value σ_c is determined by:

$$\sigma_c = \frac{1}{f_u^2}\left[f_u g_v - 2 f_v g_u + 2\sqrt{f_v g_u (f_v g_u - f_u g_v)}\right]$$

This represents the minimum ratio of inhibitor-to-activator diffusion required to trigger an instability.

1.2 | Analysis of the Dispersion Relation

The purpose of 1.1 in my work is to visualize the linear growth rate $\lambda(\Lambda)$ as a function of the Laplacian eigenvalues Λ_α. By performing a spectral decomposition for different values of ϵ and σ. The growth rate is given by the upper branch of the characteristic equation:

$$\lambda(\Lambda) = \frac{1}{2}\left[(f_u + g_v + \epsilon\Lambda(1+\sigma)) + \sqrt{(f_u - g_v + \epsilon\Lambda(1-\sigma))^2 + 4 f_v g_u)}\right]$$

- **Meaning of the plot:** It identifies the "unstable range" of eigenvalues where $Re(\lambda) > 0$. Any mode α whose eigenvalue Λ_α falls in this range will grow exponentially, leading to pattern formation.
- **The role of ϵ:** I used ϵ to shift the network's discrete eigenvalues across this unstable region.

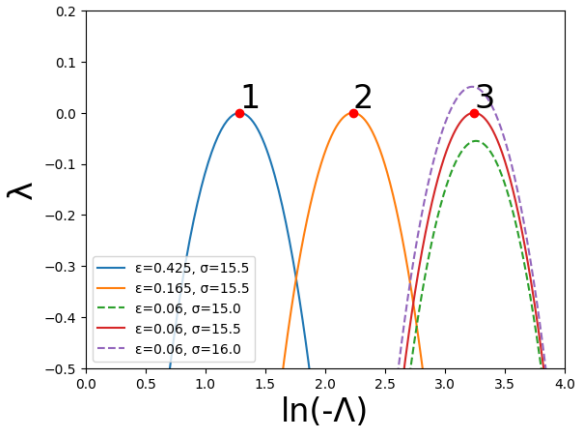

Figure 1.1: $\ln(-\Lambda)$ v growth rate λ for different σ and ϵ

1.3 | Eigenvector Localization and Structural Patterns

When a Turing pattern starts to grow after slightly exceeding the instability threshold, the activator and inhibitor distributions in this pattern are determined by the critical Laplacian eigenvector, in 1.3 we can see the critical eigenvectors for two values of diffusion constant ϵ .

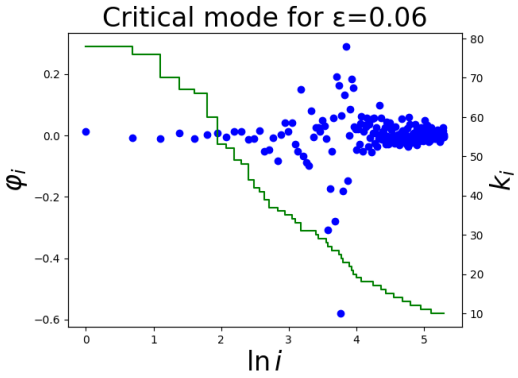

Figure 1.2: $\epsilon = 0.06$, only a subset of hub nodes undergoes differentiation

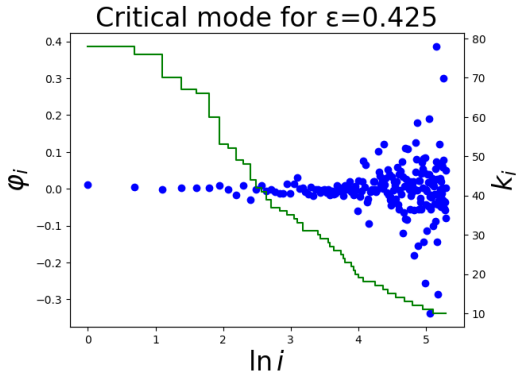

Figure 1.3: $\epsilon = 0.425$, differentiated nodes have just a few links

The visualization of the critical eigenvectors 1.3 reveals a spontaneous differentiation of nodes. There is a distinct correlation between the node degree and the amplitude of the eigenvector:

- For low mobility ϵ, the pattern localizes on hub nodes (high degree).
- For high mobility ϵ, the pattern localizes on peripheral nodes (low degree).

The differentiated nodes, with significant deviations of the activation level, tend to have close degrees, this effect is shown in 1.4 where all nodes are devided in groups for each degree and the number of differentiated nodes is counted. We can see that differentiated nodes are located along the diagonal indicating the relation between k_α and Λ_α such as k_α = - Λ_α, which leads to the following one $k_\alpha \propto 1/\ \epsilon$

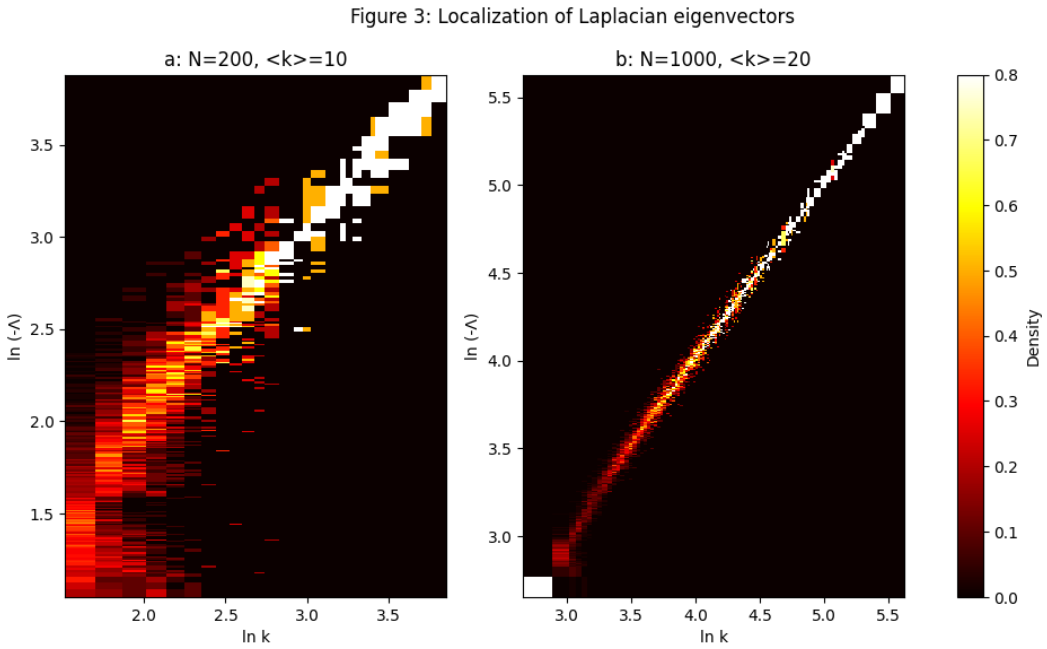

Figure 1.4: ln(k) vs ln($-\Lambda$)

1.4 | Node differentiation and hysteresis

Following the initial linear growth, the system enters a nonlinear regime, leading to asymptotic stationary states (Figure 4). The time evolution shows that while the initial pattern resembles the critical eigenvector, the final stationary state is strongly reshaped by nonlinearities. The nodes effectively segregate into two distinct groups: an activator-rich group and an activator-poor group. The "kicked-off" nodes—those deviating from the uniform background—are typically those with specific degrees, while the majority of nodes remains near the background state.

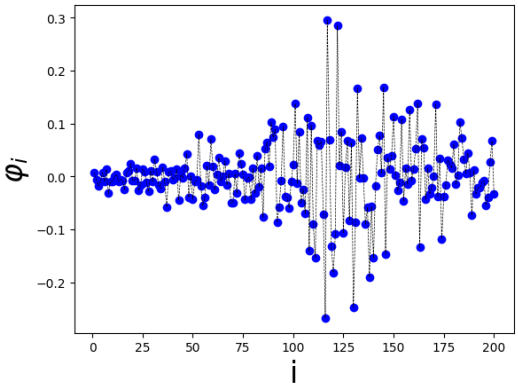

Figure 1.5: eigenvectors for each node

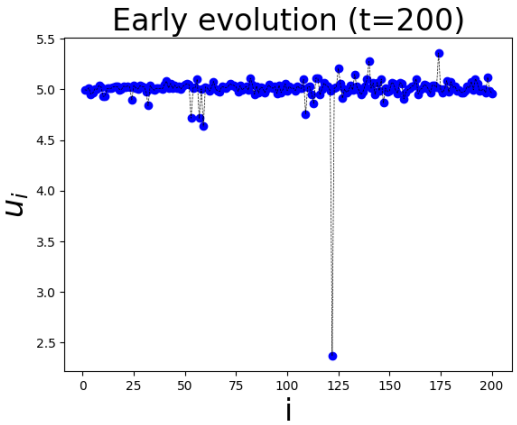

Figure 1.6: evolution of concentration u at t = 200

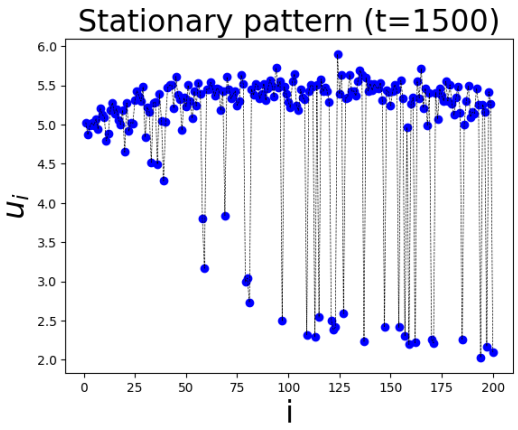

Figure 1.7: evolution of concentration u at t = 1500

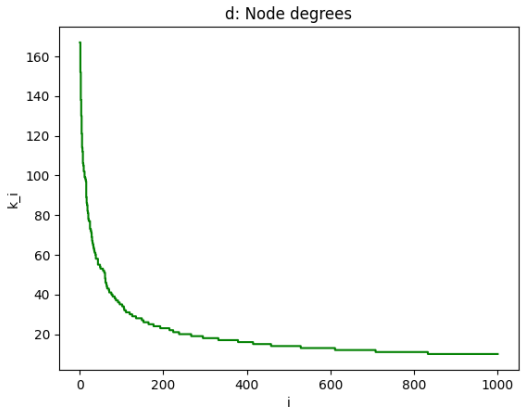

Figure 1.8: degree distribution

This differentiation process is subject to hysteresis and multistability, as detailed in 1.9. By varying the diffusion ratio σ adiabatically, we analyze the amplitude of the Turing pattern A. The plots reveal:

1. **Discontinuous Transitions:** Sudden jumps in amplitude occur at critical σ values, indicating subcritical bifurcations.
2. **Hysteresis Loops:** The path taken by increasing σ differs from the decreasing path, indicating the coexistence of multiple stable stationary patterns for the same parameters.
3. **Multistability:** Distinct branches correspond to different numbers of differentiated nodes.

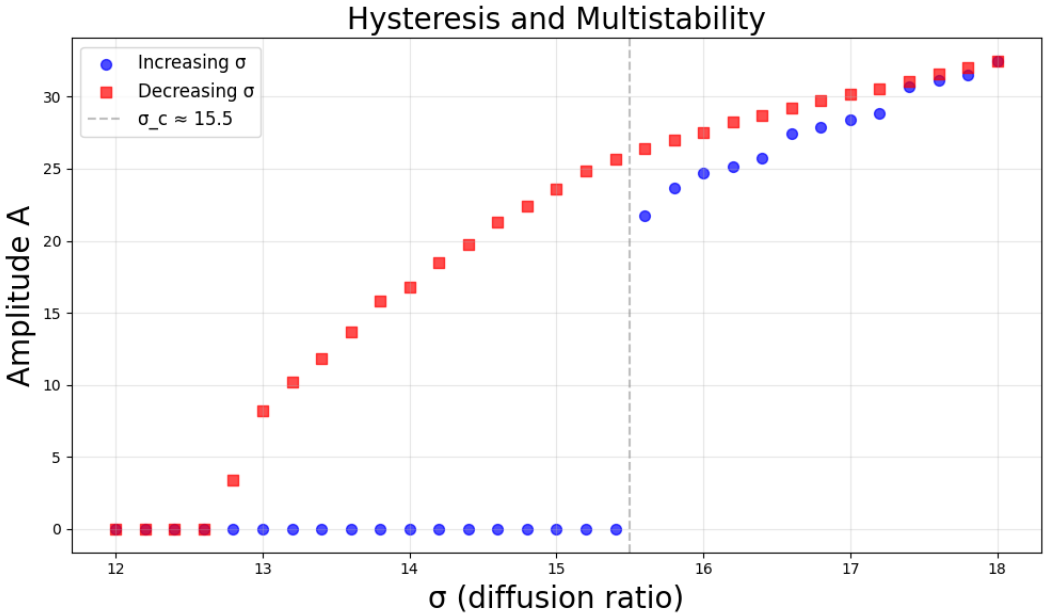

Figure 1.9: Hysteresis effect

1.5 | Mean-Field Theory Validation

Similarly to the article ref article, i tried to validate the use of mean-field approximation, this is accomplished by viewing nodes as being coupled to global mean fields $(H^{(u)}, H^{(v)})$ rather than looking at their neighbors where the coupling strength is proportional to the node degree k_i. So i preceeded to numerically calculate the densities after t iterations and ended up with similar results showing bifurcation brenches, the original article also shows stable and unstable solutions.

This demonstrates that the complex high-dimensional dynamics of the network Turing patterns can be effectively reduced to the study of a single element coupled to a global mean field, where the node degree serves as a bifurcation parameter.

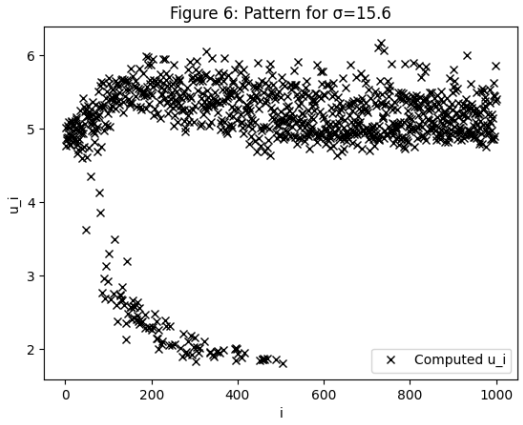

Figure 1.10: bifurcation with mean field approach for $\sigma = 15.6$

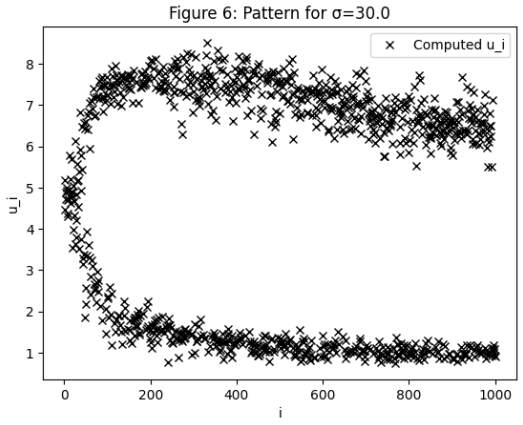

Figure 1.11: bifurcation with mean field approach for $\sigma = 30$

1.6 | Topological Extensions and perturbation analysis

The theoretical derivation presented in [3] was conducted without specific assumptions regarding the underlying topology, suggesting that the emergence of the bifurcation constitutes a general phenomenon. Indeed, analogous results were obtained in [2], where the analysis was extended to small-world networks. I extended the original study to Erdős-Rényi (ER) and Stochastic Block Models (SBM).

- **ER Networks:** Since degrees are concentrated around the mean $\langle k \rangle$, the Laplacian spectrum is narrower. I observed that the resulting patterns are more delocalized compared to the BA case 3.2, as there are no extreme hubs to "pin" the instability.
- **SBM Networks:** I utilized the community structure to see if patterns respect block boundaries. Observations reveal markedly enhanced differentiation yielding two distinctly separated communities 1.14

Following the initial differentiation, the network was perturbed by removing a fraction $p = N/5$ of its nodes. I compared the effects of a stochastic (random) removal against a targeted attack on the network's hubs on differetiated states which were

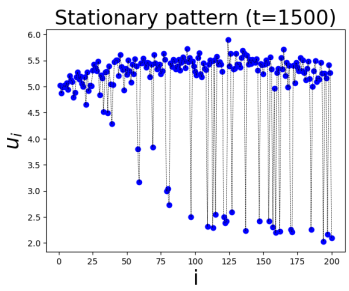

Figure 1.12: BA

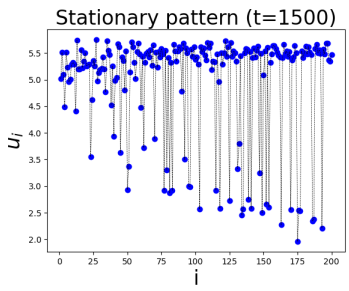

Figure 1.13: ER

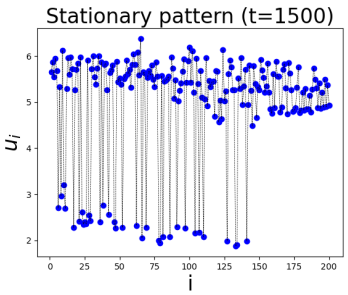

Figure 1.14: SBM

achieved after 500s, and showed the effect of the perturbations after another 1000s . In the case of Erdős-Rényi (ER) networks, the impact on the mean concentration $\langle u \rangle$ showed negligible deviation between random and targeted removal strategies 2.2. This resilience is consistent with the statistical homogeneity characteristic of ER topologies. A similar behavior was observed in Stochastic Block Model (SBM) networks; despite the inherent modularity dividing nodes into two distinct communities, the system's response remained comparable under both perturbation schemes 2.1.

Conversely, Barabási-Albert (BA) networks exhibited a marked sensitivity to targeted attacks. The effect of hub removal on the global dynamics was significantly more pronounced than that of random removal 2.3. This discrepancy is expected in scale-free architectures, where high-degree nodes are observed to sustain high concentrations of the variable u.

Notably, across all investigated topologies and removal strategies, the bifurcation phenomenon persisted post-perturbation. This suggests that the capacity for differentiation is a robust, intrinsic property of the system, largely independent of the specific underlying network structure.

1.7 | Conclusion

In this project, I reproduced the results obtained in [**?**], which analyzes how Turing patterns behave on networks by varying different parameters like the diffusion constant and mobility. My results are compatible with those of the authors, and I added a perturbation analysis to see if the bifurcation pattern would hold.

2 | Appendix

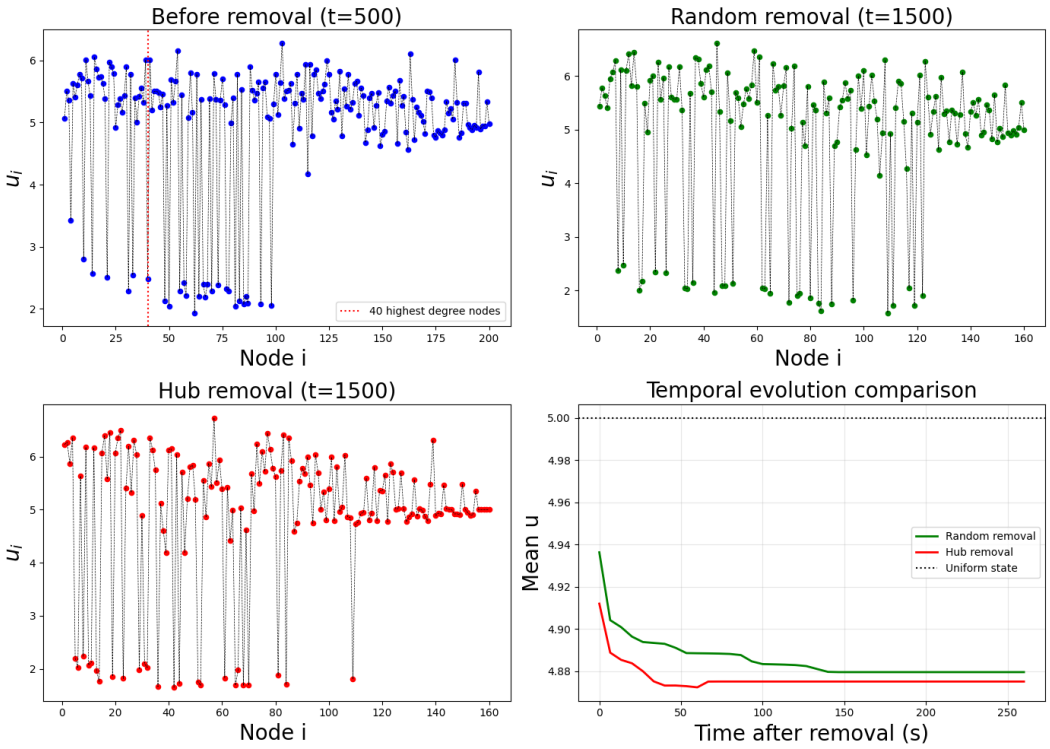

Figure 2.1: SBM

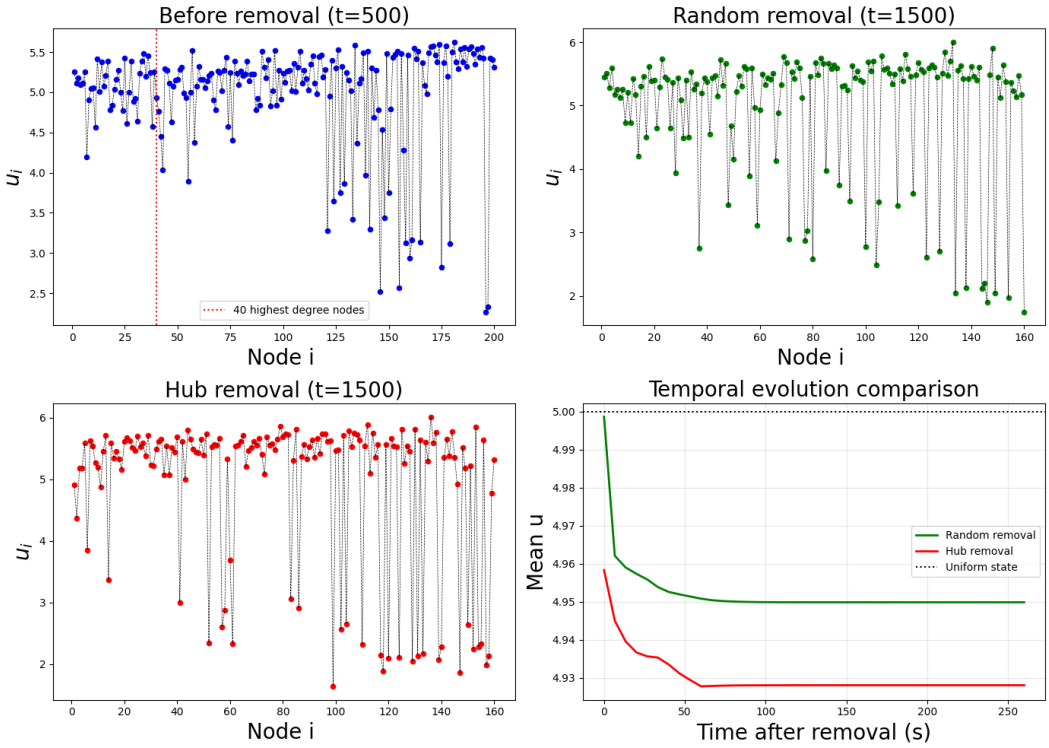

Figure 2.2: ER

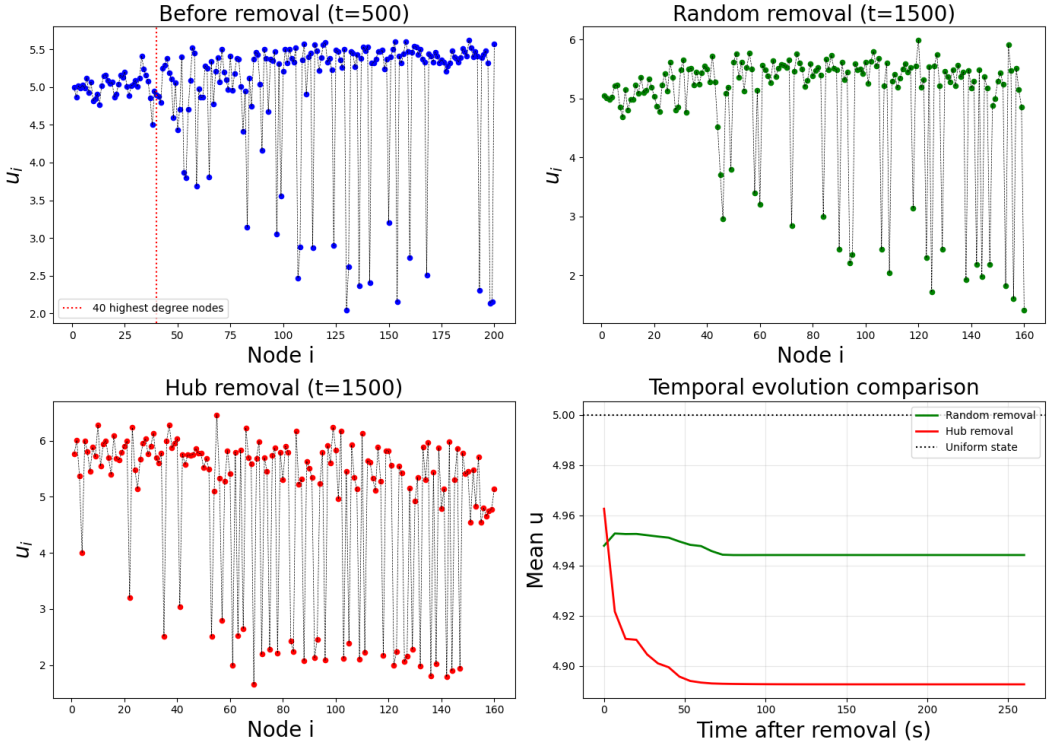

Figure 2.3: BA

3 | Network Construction for World Cities

This chapter details the methodological framework adopted to reconstruct the topological structure of public transport networks across various cities worldwide, the dataset was downloaded from [1]. The procedure was implemented using Python, leveraging the `pandas` library for data manipulation and `networkx` for graph analysis. The workflow proceeds through three distinct phases: data pre-processing, topological inference, and global scaling analysis.

3.1 | Data Pre-processing and Node Definition

The primary input for the network construction consisted of raw datasets containing information on transport stations, city identifiers, and transit lines. The initial phase involved a rigorous data cleaning process on the source file `stations.csv`. Entries containing malformed delimiters or non-numeric identifiers were programmatically detected and removed to ensure data integrity.

Subsequently, the station data was merged with `cities.csv` and `cityline.csv` to associate every station with its respective metropolitan area and transit line. This aggregated dataset was then grouped by `city_id`. For each specific city, a distinct dataset was generated and saved in the `network_nodes` directory. In this formalism, every station represents a **node** (v) in the city's graph G.

3.2 | Edge Reconstruction and Index Remapping

The connectivity of the network (edges) was inferred from the sequence of stations within specific transit lines. For every city, the algorithm filtered the transit data to isolate lines associated with that metropolitan area.

Stations were sorted based on their sequence within a line. An **edge** (e) was established between any two stations i and $i+1$ that appear consecutively in the transit sequence. To accurately represent the bidirectional nature of transport infrastructure, edges were generated as directed links in both directions (Source $\rightarrow$ Target and Target $\rightarrow$ Source). These connections were archived in city-specific CSV files within the `network_edges` directory.

To facilitate matrix operations and computational analysis, a remapping proce-

dure was applied. The original, often non-contiguous station identifiers were mapped to a contiguous range of integers $[0, N-1]$, where N is the total number of stations in the city. This normalization step yielded two final sets of standardized files:

- **Remapped Nodes:** Containing the station metadata and new integer IDs.
- **Remapped Edges:** Containing the source-target pairs corresponding to the new IDs.

3.3 | Global Scaling Analysis

Following the reconstruction of the individual city networks, a comparative analysis was performed to investigate the relationship between the network size and its connectivity. For every city c, the total number of stations (N_c) and the total number of physical connections (E_c) were computed.

To characterize the topological scaling of these infrastructure networks, I modeled the relationship between edges and nodes using a power law:

$$E \propto N^{\beta} \tag{3.1}$$

By transforming this relationship into a log-log scale, I performed a linear regression analysis across the global dataset.

Figure 3.3 illustrates the result of this analysis. The scatter plot represents the distribution of cities in the $N - E$ plane. The regression yields a scaling exponent (slope) of $\beta \approx 1.056$. This super-linear behavior suggests that as public transport networks grow in size (number of stations), the complexity of connections increases at a slightly faster rate than the simple addition of nodes, implying a densification of the network structure in larger metropolitan systems.

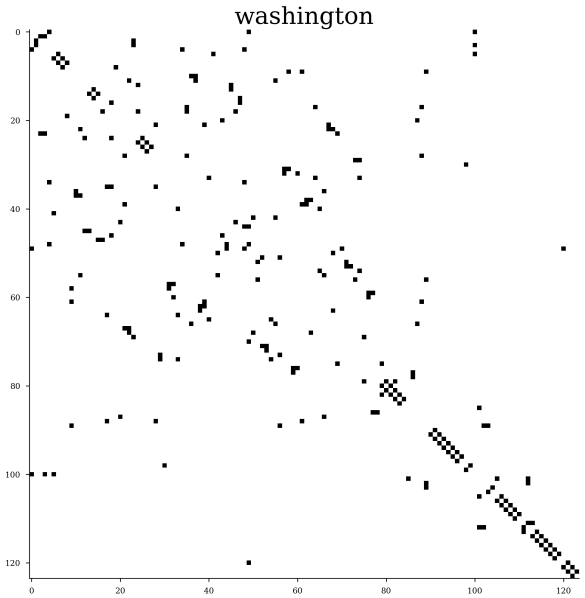

Figure 3.1: Washington pulic transport matrix

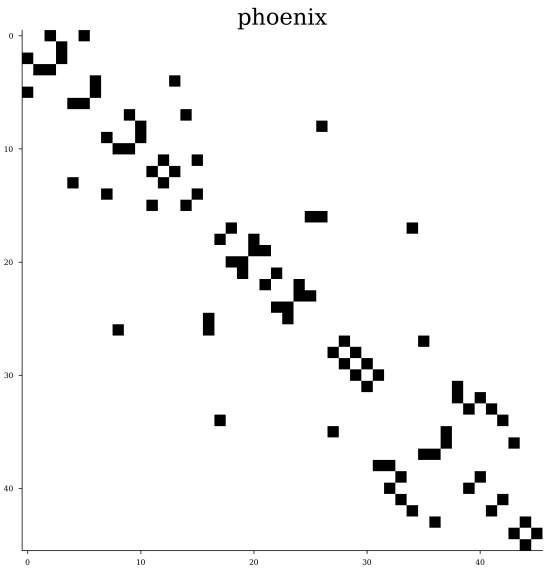

Figure 3.2: Phoenix pulic transport matrix

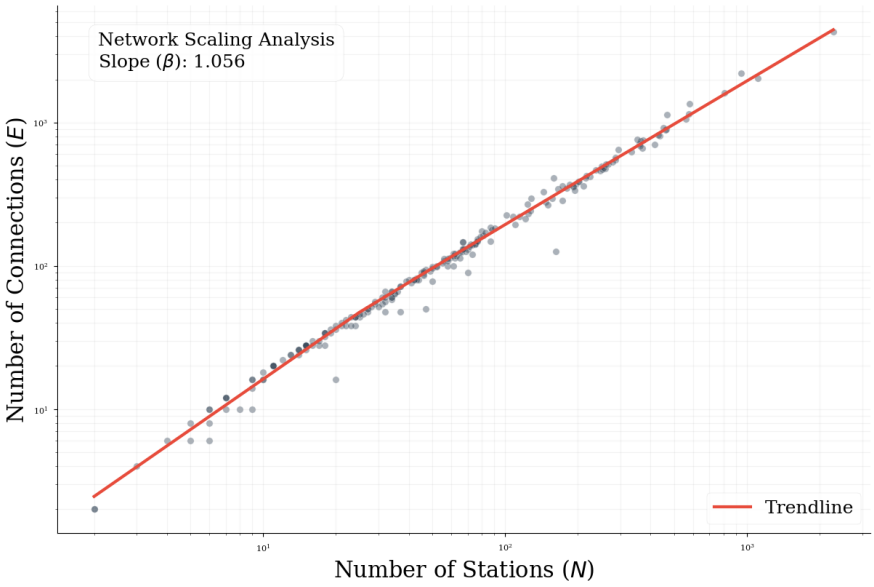

Figure 3.3: Scaling relationship between the number of stations (N) and the number of links (E) for public transport networks worldwide. The regression line (red) indicates a scaling exponent $\beta \approx 1.06$, plotted on a log-log scale.

4 | Bibliography

[1] Citylines.co. Citylines open data portal, 2024.

[2] Riccardo Muolo, Lorenzo Giambagli, Hiroya Nakao, Duccio Fanelli, and Timoteo Carletti. Turing patterns on discrete topologies: from networks to higher-order structures. *Proceedings of the Royal Society A: Mathematical, Physical and Engineering Sciences*, 480(2302):20240235, 2024.

[3] Hiroya Nakao and Alexander S. Mikhailov. Turing patterns in network-organized activator–inhibitor systems. *Nature Physics*, 6(7):544–550, 2010.